PAPER

Check for updates

Cuttlefish ink nanoparticles-integrated aerogel membranes for efficient solar steam generation†

Yong Liu, [iD] *[a] Ruyue Wang,[a] Kaiyuan Wang,[a] Fei Yang,[a] Yundi Chen,[a] Wenwen Xie,[a] Shengxu Luo, [iD] *[a] Zhenyi Liang,[a] Qian Wang*[c] and Juanjuan Li [iD] *[b]

Solar steam generation is a promising technology to obtain freshwater from seawater and sewage. Photothermal materials play an essential role in solar evaporators. Existing materials used to fabricate solar evaporators usually suffer from environmental concerns due to the use of hazardous chemicals or their inability to degrade. This work presents a fully biomass-derived aerogel membrane as a solar absorber for interfacial evaporation. The aerogel is made of an aga matrix doped with cuttlefish ink nanoparticles (CFNPs), using a freezing-assisted solvent displacement method. Under 1 sun irradiation, the CFNPs@Aga aerogel membrane shows an ultrahigh evaporation rate of 3.06 kg m^{-2} h^{-1} with a light-to-vapor energy efficiency of 94.91%. The solar evaporator can produce freshwater from both simulated and real samples of seawater. The evaporator possesses excellent salt self-cleaning performance, and is easily degradable and highly cost-effective. These results provide a green sustainable solution for solar energy conversion and water purification.

Sustainability spotlight

This study provides a green strategy for high-efficiency utilization of solar energy to obtain clean water from seawater and sewage. Our research aligns with UN Sustainable Development Goals (SDGs) 6 (Clean Water and Sanitation), 7 (Affordable and Clean Energy), and 14 (Life below Water). High-efficiency solar absorbers are critical for solar energy collection and conversion. Existing materials to fabricate solar absorbers suffer from environmental concerns due to the use of hazardous chemicals or their inability to degrade. We designed a fully marine biomass-derived solar absorber using cuttlefish ink nanoparticles combined with the aga hydrogel (SDG 14). A solar evaporator was devised for photothermal energy conversion that drives interfacial water evaporation (SDG 7). The solar evaporator can produce freshwater from both simulated and real samples of seawater (SDG 6). Overall, our work highlights the potential of marine resources in producing valuable materials for energy conversion and sustainable development.

Introduction

Solar-driven interfacial evaporation, an emerging solar-thermal technology that heats water at the air/liquid interface for promoted vaporization, has driven global applications in seawater desalination and sewage purification.[1,2] Solar absorbers, which are implemented using various photothermal materials, represent the first critical step to convert light to heat and drive steam generation.[3] These light absorbing materials are immobilized on or embedded in bulk matrices with designed evaporation structures to work cooperatively as a complete interfacial evaporator. Despite the numerous designs of evaporators, little attention has been paid to the

[a]School of Chemistry and Chemical Engineering, Hainan University, Haikou 570228, China. E-mail: liuyong@hainanu.edu.cn

[b]School of Life Sciences, Hainan University, Haikou 570228, China. E-mail: lijuanjuan@hainanu.edu.cn

[c]College of Materials Science and Engineering, Taiyuan University of Technology, Taiyuan 030024, China. E-mail: qianwang0825@pku.edu.cn

† Electronic supplementary information (ESI) available. See DOI: https://doi.org/10.1039/d3su00301a

environmental concerns that may accompany the full lifetime of the evaporation devices, from their fabrication, service, and retirement, to their harmless treatment.

Synthetic solar absorbers, which are typically carbonaceous materials,[4] plasmonic particles,[5] semiconductors,[6,7] metal oxides,[8] MXene,[9] and so forth, have generally encountered at least one of the following problems: very high energy consumption, tedious preparation, usage or production of hazardous chemicals, high cost, poor degradability, and potential environmental toxicity. For example, photothermal materials containing metal elements such as iron (Fe), copper (Cu), cobalt (Co), silver (Ag), *etc.*, inevitably suffer from metal ion leakage that causes aquatic or pedologic toxicity. The above problems may also occur with host materials supporting the photothermal absorbers if synthetic polymers or plastic sponges are used.[10] For example, polymeric materials (including hydrogels) containing fluorine (F) and boron (B) are difficult to degrade in the environment and can cause adverse ecological impacts. Balancing the evaporation performance and the environmental friendliness (green manufacturing, ecological safety, degradability, *etc.*) is thus important for designing next-

generation evaporators. Since the environmental fate of synthetic materials is difficult to accurately predict, harnessing natural resources to construct functional materials paves another road toward sustainability. Compared to synthetic chemicals, materials derived from natural resources provide improved safety and sustainability. However, there is still much room for developing fully biomass-derived solar absorbers for interfacial evaporation.

Cuttlefish, a marine animal, can eject a black, inklike fluid when faced with danger. Cuttlefish inks are rich in the pigment melanin, which is known to have excellent photothermal conversion capacity.[11] As a natural bioresource, cuttlefish inks provide a renewable resource pool for developing solar absorbers.[12] Recently, hydrogels with three dimensional (3D) porous structures and abundant hydrophilic functional groups have been shown to benefit the evaporation process through reducing the evaporation enthalpy of water.[13] However, hydrogels tend to lose water in ambient conditions, complicating their long term preservation and usage.[14] Aerogels, which are typically obtained from hydrogels by replacing water with air, preserve their original 3D structures and can absorb water to remodel hydrogel-like structures. Thus, aerogels provide an ideal platform for evaporator design.[15,16]

Herein, we extracted photothermal nanoparticles from cuttlefish ink (cuttlefish ink nanoparticles, CFNPs) and embedded them in an aerogel matrix as a membrane-type solar absorber for interfacial evaporation (Fig. 1). Like the CFNPs, the aerogel was fabricated from a marine biomass-derived material, agar powder, through solvent exchange and air drying of the formed organogel. Compared to lyophilization, the solvent exchange method saved a great deal of time and energy for preparing aerogels.[17] We avoided the use of metallic materials, synthetic polymers, toxic organic solvents, and other hazardous chemicals throughout the synthetic process. The composite aerogel CFNPs@Aga achieved a high evaporation rate of 3.06 kg $m^{-2} h^{-1}$ under 1 sun irradiation, and were successfully applied in extracting freshwater from simulated seawater and dye-contaminated sewage. The aerogel undergoes fast degradation in hot alkaline solution. Our results highlighted the efficient utilization of marine resources for material development toward obtaining freshwater.

Experimental section

Materials and chemicals

Cuttlefish ink sacs were collected from a fish market. Aga powder (A. R.) was from Solarbio. Ultrapure water was produced using a UPR-II-10TNZ ultrapure water system (Sichuan ULU-PURE, China). Eriochrome black T (A. R.) was from Macklin. Sodium chloride (A. R.) was from Guangzhou Chemical Reagent Factory. Ethanol absolute (A. R.) was from Sinopharm Chemical Reagent Co., Ltd. *P. aeruginosa* was kindly donated by Professor Zhu Liu's group and was cultured in Luria–Bertani (LB) medium.

Characterization

Ultraviolet-visible (UV-Vis) absorption spectra were obtained using a UV-Vis spectrophotometer (UV-2600, Shimadzu). For example, a solution of CFNPs diluted to a suitable concentration was placed in a quartz cuvette, and the spectrum was measured in the range of 300–800 nm, using ultrapure water as a control (scanning speed: medium speed; sampling interval: 0.2 nm). Optical microscopy images were obtained using a positive fluorescence microscope (DM5000B, Lycra). Scanning electron microscope (SEM) images were obtained using a field emission SEM (FESEM, VeriosG4UC, Thermo Fisher Scientific). Total dissolved solids (TDS) were measured using a conductivity meter (DDSJ-308-a, Rex). Samples were placed in 50 mL plastic tubes and measured in TDS mode with a calibrated electrode. X-ray photoelectron spectroscopy (XPS) was conducted using an
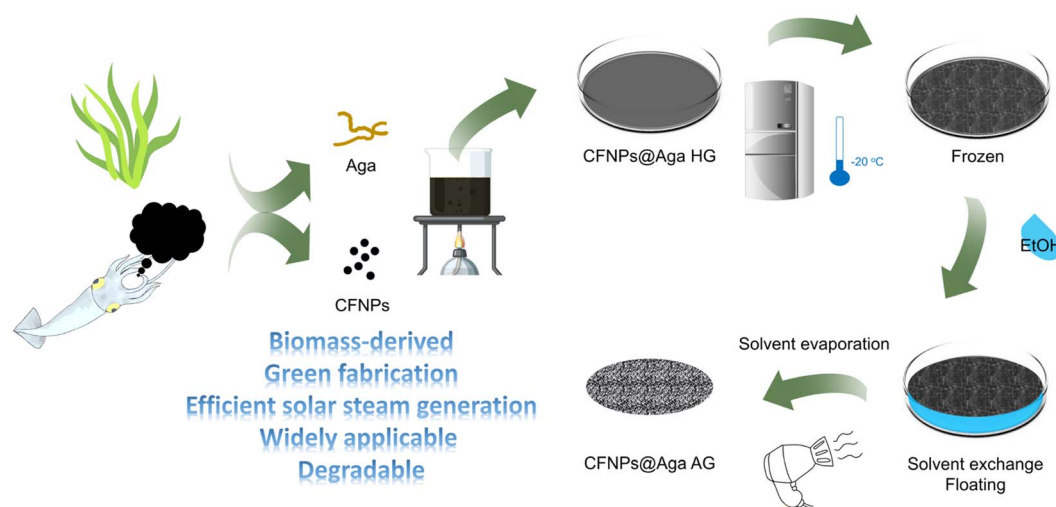

Fig. 1 Design and preparation of the CFNPs@Aga aerogel membrane as the evaporation interface. The CFNPs are extracted from cuttlefish inks and doped into the aga solution to form the CFNPs@Aga hydrogel (HG). The hydrogel is frozen and then subjected to solvent replacement using ethanol. Finally, the organogel is dried in the air to form the CFNPs@Aga aerogel (AG).

XPS spectrometer (Thermo ESCALAB 250XI). Fourier transform infrared spectroscopy (FTIR) spectra were recorded using an IR spectrometer (Nicolet iS 10). Differential scanning calorimetry (DSC) was performed using a differential scanning calorimeter (Mettler, DSC3). Inductively coupled plasma-optical emission spectroscopy (ICP-OES) was conducted with an ICP-OES spectrometer (PerkinElmer 8300).

Extraction of nanoparticles from the cuttlefish ink (CFNPs)

The cuttlefishes used in this work belonged to the family Ommastrephidae (Fig. 2a). The collected cuttlefish ink sacs were cut into pieces and washed repeatedly with ultrapure water. The solution was centrifuged at 2000 rpm for 3 min and the precipitate was discarded. The upper solution was further centrifuged at 9000 rpm for 10 min to obtain the black precipitate, which was then dispersed in ultrapure water as the stock solution of CFNPs. To determine the weight concentration of CFNPs, 500 µL of nanoparticle solution was centrifuged and dried overnight in an 80 °C oven, and the collected powder was weighed using an analytical balance to estimate the concentration.

Preparation of the CFNPs@Aga aerogel

In a typical synthesis, 340 mg agar powder was dissolved in 20 mL ultrapure water by heating it to boiling. After cooling slightly, 3.5 mL of the agar solution was transferred to a plastic tube and mixed with 0.5 mL CFNPs solution (the concentration was determined to be 8 mg mL^{-1}) to reach a doping concentration of 1 mg mL^{-1}. The mixed solution was poured into a plastic dish with a diameter of 30 mm and allowed to form a hydrogel upon cooling at room temperature. The aga solution without CFNPs was used as the control to prepare the aga hydrogel. The hydrogel sample was placed in a refrigerator at −20 °C for 2 hours; subsequently, 2 mL anhydrous ethanol was immediately added to immerse the frozen hydrogel for solvent exchange. After 0.5 h, the organogel was taken out and dried with a hair dryer to obtain the aerogel.

Fabrication of the evaporator and its evaporation performance

The evaporator comprised a 50 mL plastic beaker for loading water samples, a polyurethane foam thermal insulation tank, a CFNPs@Aga aerogel for interfacial evaporation, and a paper string for water delivery. A small hole was cut at the bottom of the foam to assemble the paper string, and the distance between the evaporation interface and the water level was ∼3 cm.

To measure the evaporation rate, ∼30 mL ultrapure water was added to the beaker and the evaporator was placed on an analytical balance. A xenon lamp (CHF-XM500, PerfectLight, Beijing) was applied as the stimulated sunlight irradiation (the intensity was set as 1 sun, ∼1000 W m^{-2}). The weight of the whole evaporator was recorded continuously for 1 hour at time points of 0, 5, 10, 15, 20, 30, 40, 50, and 60 min. Meanwhile, the temperature changes at the evaporation interface were recorded using an infrared camera (HM-TPH16-6VF/W, HIKVISION).

To test the cycling performance and durability of the evaporator during repeated use, the evaporator was used to treat 5.0 wt% NaCl solution. The experiment was repeated three times using the same piece of CFNPs@Aga aerogel membrane, and the evaporation rate in each cycle was measured and compared.

Treatment of simulated seawater and sewage

The evaporator was placed on a glass Petri dish and covered with a 200 mL beaker to serve as the condensation system. NaCl solutions of 0.8 wt% and 3.5 wt% were used to simulate seawater with different salinities. The NaCl solution was added to the evaporator and the device was irradiated with the lamp for 4 h to collect freshwater. The TDS value was measured before and after evaporation to evaluate the desalination performance. A 5 mg mL^{-1} solution of Eriochrome black T EBT was used to simulate dyeing wastewater. The absorption spectra of the samples before and after treatment were measured and compared (samples were diluted 10 times). *Pseudomonas aeruginosa* (*P. aeruginosa*) cells dispersed in phosphate buffer saline (PBS) at 10^9 to 10^{10} CFU mL^{-1} were used as simulated sewage with bacterial pathogens. Bacterial numbers in samples before and after treatment were determined using the plate counting method.
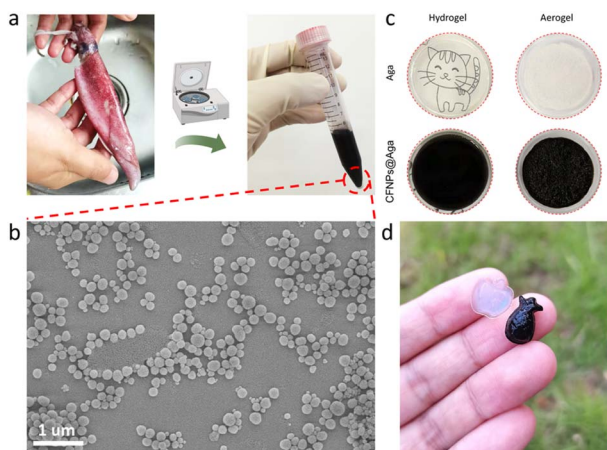

Fig. 2 CFNPs@Aga hydrogel and aerogel. (a) Extraction of CFNPs from cuttlefish. (b) SEM image of CFNPs. (c) Photographs of aga hydrogel/aerogel and CFNPs@Aga hydrogel/aerogel. (d) Hydrogels with different shapes.

Salt self-cleaning performance of the CFNPs@Aga aerogel

The evaporator was assembled as described in "Fabrication of the evaporator and its evaporation performance". Then, 0.1 g of NaCl crystals was placed on the top of the evaporator, and photographs were taken at different timepoints to monitor the remaining NaCl on the aerogel membrane.

Degradability and ecological impact of the CFNPs@Aga aerogel

The aga aerogel and CFNPs@Aga aerogel were cut into sector-shaped pieces and immersed in 1 M NaOH heated by an 80 °C water bath. The samples were imaged at 0 and 2 h to estimate the degradation progress.

To study the aquatic toxicity of the composite aerogel, *Poecilia reticulata* was cultured with aga, CFNPs@Aga, and CFNPs for 7 days. The fish were photographed at day 1, 3, and 7 to assess their activity. To study the natural degradation of CFNPs@Aga membranes in the soil, three pieces of membrane were weighed and buried in the soil. After 14 days, the samples were collected, washed, dried, and weighed again to calculate the degradation efficiency.

Desalination of real seawater samples

Seawater was collected from Nandu River, Haikou and was directly used for purification. Briefly, the sample was loaded in the evaporator equipped with a condensation system and a collector (see Fig. 7a). The whole device was placed under sunlight from 8:00 am to 18:00 pm. The mass change of the evaporator, the air temperature, and the sunlight intensity were continuously recorded.

Evaluation of the photothermal properties of CFNPs

The CFNPs were dispersed in ultrapure water (0.1 mg mL^{-1}). Then, 200 μL of the CFNPs solution was moved to a 1.5 mL EP tube, and the tube was irradiated with an 808 nm laser at 1 W cm^{-2} for 10 min. Ultrapure water was used as the control. The temperature of the solution was continuously monitored using an IR imaging system (FOTRIC 220 s). After 10 min, the laser was shut off, and the cooling temperature curve was monitored for another 10 min. To evaluate the photothermal stability of the CFNPs, three on–off cycles were applied to the solution (laser on for 5 min, off for 3 min) and the temperature was monitored.

Calculation of the photothermal conversion efficiency

During the photothermal conversion process, the energy balance can be expressed as

$$m_s C_{p,s} + m_c C_{p,c} \frac{d\Delta T}{dt} = Q_{input} - Q_{loss} \tag{1}$$

where $m_s = 0.2$ g is the mass of the solution, $C_{p,s} = 4.2$ J g^{-1} K^{-1} is the constant-pressure heat capacity of the solution, $m_c = 0.085$ g is the estimated mass of the irradiated area of the container, $C_{p,c} = 1.9$ J g^{-1} K^{-1} is the heat capacity of the container, ΔT is the difference between the solution temperature T at time t and the starting solution temperature T_0 ($T_0 = T_{surr}$, where T_{surr} is the temperature of the surrounding environment), Q_{input} is the energy input by the laser illumination, and Q_{loss} is the energy dissipated to the surrounding environment. Q_{input} can be further expressed as

$$Q_{input} = I(1 - \xi)(1 - 10^{-A_\lambda})\eta + I\xi \tag{2}$$

where ξ is the fraction of the laser energy absorbed by the container walls and the solution of CFNPs, $I = 0.20$ W is the laser power exerted on the system, $A_\lambda = 0.78$ is the extinction value at the illumination laser wavelength (808 nm), and η is the photothermal conversion efficiency of the CFNPs. The energy dissipation typically occurs through heat conduction and thermal radiation, and can be expressed as

$$Q_{loss} = B\Delta T \tag{3}$$

where B is the unknown coefficient. Combining eqn (1)–(3), we obtain

$$m_s C_{p,s} + m_c C_{p,c} \frac{d\Delta T}{dt} = I(1 - \xi)(1 - 10^{-A_\lambda})\eta + I\xi - B\Delta T \tag{4}$$

The unknown parameter B was determined by switching off the laser when the temperature rise reached a plateau. Under this condition, eqn (4) becomes

$$m_s C_{p,s} + m_c C_{p,c} \frac{d\Delta T}{dt} = -B\Delta T \tag{5}$$

During the cooling process, $\Delta T = T - T_{surr}$. Eqn (5) thus becomes

$$m_s C_{p,s} + m_c C_{p,c} \frac{dT}{dt} = -BT + BT_{surr} \tag{6}$$

Integrating T with respect to t (note that at $t = 0$, $T = T_{max}$, where T_{max} is the highest temperature reached upon heating), we obtain

$$T = (T_{max} - T_{surr})e^{-\frac{Bt}{M}} + T_{surr} \tag{7}$$

The parameters and constants involved in eqn (7) are listed below

	Description	Value
B	Unknown parameter	—
M	Constant, $M = m_s C_{p,s} + m_c C_{p,c}$	1.0 J K^{-1}
T_{max}	Constant	50.9 °C
T_{surr}	Constant	27.5 °C

Through fitting the temperature decay curve, we obtain $B = 0.416$ J K^{-1} min^{-1}.

ξ is determined by replacing the CFNPs solution with water. Eqn (4) becomes

$$m_s C_{p,s} + m_c C_{p,c} \frac{d\Delta T}{dt} = I\xi - B\Delta T \tag{8}$$

When the temperature rise reaches the steady state, the left side of eqn (8) becomes zero. ξ was determined from the end temperature to be 0.013.

After the parameters B and ξ are known, the photothermal conversion efficiency is obtained by

$$\eta = \frac{B(T_{\max} - T_{\text{surr}}) - I\xi}{I(1 - \xi)\left(1 - 10^{-A_\lambda}\right)}$$

The η of the CFNPs solution was determined to be 24.5%.

Results and discussion

Fabrication and characterization of the CFNPs@Aga aerogel

The CFNPs@Aga aerogel was prepared in five steps: mixing, gelation, freezing, solvent exchange, and drying; these procedures are detailed in the Experimental section. The melanin-like structure of the CFNPs, which comprised abundant hydrophilic phenolic groups, made them facile to integrate with the aga matrix.[18] During solvent exchange, the ice crystals that occupied the pores in the hydrogel melted and were replaced with ethanol molecules, which were more easily removed compared to water molecules in the subsequent air-drying process. Consequently, the organogel turned into the aerogel. The total time for preparing the aerogel membrane was 4 h, which was much shorter than that for many other synthetic solar absorbers. The extracted CFNPs was black in appearance (Fig. 2a) and were found to be monodispersed particles under scanning electron microscope (SEM) observation, with an average size of 134 nm (Fig. 2b and S1†). As a result, the aga hydrogel/aerogel turned from pale yellow to deep black after doping with CFNPs (Fig. 2c). Due to the temperature-responsive gelation behaviour of agar, the hydrogel (as well as the aerogel) was highly designable in size and shape to meet the requirements for different application scenarios (Fig. 2d).

We studied the chemical and morphological structures of the CFNPs and composite aerogels. The ultraviolet-visible (UV-Vis) absorbance spectrum of the CFNPs exhibited a broad absorption band from ∼300 to ∼800 nm, which corresponded well with the reported melanin structures and might benefit the photothermal conversion process of the aerogel upon solar irradiation (Fig. 3a).[19] Fourier transform infrared spectroscopy (FTIR) showed that the CFNPs@Aga composite had three characteristic peaks/bands at 1040, 1645, and 3000–3700 cm^{-1}. Compared to the FTIR spectra of the aga powder CFNPs, these peaks/bands confirmed the successful blending of CFNPs and aga in the composite aerogel (Fig. 3b). The exact chemical structures of the CFNPs remain unknown, but are believed to comprise melanin-like structures.[20,21] The molecular structures of the aga and melanin units are shown in Fig. 3c. It was noted that the O–H peak (3000–3700 cm^{-1}) shifted to lower wavenumber and became broader in the aerogel, suggesting the formation of hydrogen bonds between aga and CFNPs (possibly through interactions between hydroxyl groups).

We also characterized the unpurified cuttlefish ink solution (CF) using SEM and FTIR. Compared to the extracted CFNPs, the CF sample appeared pasty under SEM observation, with closely stacked CFNPs embedded in a complex medium possibly composed of various biomolecules (Fig. S2†). FTIR analysis showed negligible differences between the CFNPs and
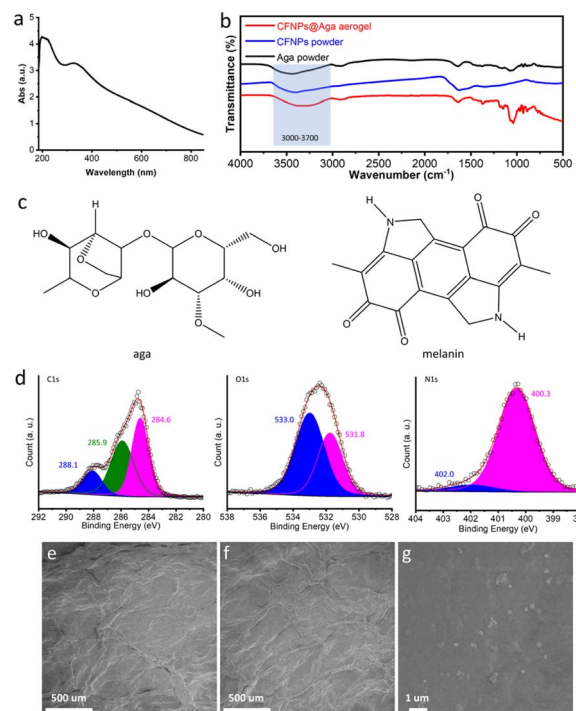

Fig. 3 Chemical and morphological characterizations of CFNPs and the CFNPs@Aga aerogel. (a) UV-Vis absorption spectrum of CFNPs. (b) FTIR spectra of aga, CFNPs, and the CFNPs@Aga aerogel. (c) Molecular structures of aga powder and the melanin unit. (d) Detailed XPS spectra (C 1s, O 1s, and N 1s) of CFNPs. (e–g) SEM images of the aga aerogel (e) and the CFNPs@Aga aerogel (f and g).

CF samples (Fig. S3†), indicating that CFNPs were the major component of CF.

X-ray photoelectron spectroscopy (XPS) spectra of the CFNPs confirmed the presence of the elements C (66.41%, atomic ratio), O (24.53%), and N (9.05%) (Fig. S4†). Detailed analysis of the C 1s spectrum revealed three components at 288.1, 285.9, and 284.6 eV. The peak at 288.4 eV was assigned to the quinone groups (C=O), which corresponded well with the 531.8 eV peak in the O 1s spectrum (Fig. 3d).[22] The peaks at 285.9 and 284.6 eV were from C–C, C=C, C–O, and C–N groups. The N 1s region was fitted with two peaks at 402.0 and 400.3 eV, which were assigned to cyclized R$_2$NH (possibly from the 5,6-dihydroxyindole (DHI) unit)[23] and free RNH$_2$ groups in the CFNPs, respectively. These results supported the melanin-like structures of the CFNPs, which were essential for their photothermal conversion properties.

The optical microscope images and SEM images confirmed the porous networks of both the agar and CFNPs@Aga aerogels (Fig. 3e and f and S5†). At higher magnifications of SEM, the CFNPs were explicitly seen to be embedded in the aerogel matrix (Fig. 3g). The CFNPs@Aga aerogel possessed a water absorption capacity of 7.67 g g^{-1} after 4 h of incubation, making it suitable for evaporation-driven water treatment (Fig. S6†). Overall, the CFNPs could be successfully doped into the aga matrix to form porous membrane structures for interface evaporation.

Photothermal performance of CFNPs and the CFNPs@Aga aerogel

We investigated the photothermal conversion properties of CFNPs using an 808 nm laser as the irradiation source. CFNPs were dispersed in water at a concentration of 0.1 mg mL^{-1} and the solution was continuously illuminated by the laser at a power density of 1 W cm^{-2}. After irradiation for 10 min, the control sample (ultrapure water) showed a negligible temperature increase (ΔT) of 1.3 °C. In contrast, the CFNPs solution exhibited a large ΔT of 23.4 °C (from 27.9 to 51.3 °C), suggesting the photothermal conversion activity of the CFNPs (Fig. 4a). Additionally, the CFNPs exhibited good stability during three on–off cycles, showing no decrease in the temperature rise value (Fig. S7†). The photothermal conversion efficiency (PCE) of the CFNPs was measured to be 24.5% after fitting the cooling temperature curve (details are included in the Experimental section, Fig. 4b). This high PCE was comparable to the highest PCE value reported for synthetic melanin structures ($\sim$25.6%),[24] suggesting the great potential of CFNPs as natural energy conversion materials.

The CFNPs@Aga aerogel was applied for interfacial evaporation under simulated solar irradiation. The evaporator was designed as shown in Fig. 4c, top. The aerogel membrane was supported using polyurethane foam to avoid direct water contact, and water transportation was realized by a "paper string" made of a daily use soft paper towel. This design allowed reduced downward thermal leakage to the underlying water and thus could maximize the utilization of thermal energy for heating the water at the interface.[25] The water delivery properties of the "paper string" were studied using an aqueous black ink (Fig. S8a†). An average transportation rate of 2.4 cm min^{-1} was achieved in the first 3 min, with a maximum of 4.1 cm min^{-1} in the first minute (Fig. S8b†).

We measured the photothermal conversion performance of the CFNPs@Aga aerogels with different doping concentrations of CFNPs (0.5 and 1.0 mg mL^{-1}). A xenon lamp with an output power of 1 sun (1000 W m^{-2}) was applied to simulate sun irradiation. Infrared (IR) images showed a significantly greater temperature increase in the CFNPs@Aga aerogels (compared to the agar aerogel) after 2 min of irradiation (Fig. 4c, bottom). The surface temperature in the different groups reached 38.1, 42.5, and 47.2 °C for the agar, CFNPs$_{0.5}$@Aga, and CFNPs$_{1.0}$@Aga aerogels, respectively. At 60 min post-irradiation, the surface temperature reached 44.4, 78.0, and 75.3 °C for agar, CFNPs$_{0.5}$@Aga, and CFNPs$_{1.0}$@Aga aerogels respectively, corresponding to a ΔT of 15.6, 51.6, and 48.9 °C (Fig. 4d). The slightly lower ΔT of the CFNPs$_{1.0}$@Aga aerogel (with a higher concentration of CFNPs) compared to that of the CFNPs$_{0.5}$@Aga aerogel was possibly attributed to the fact that the photothermal conversion reached a "saturated" state at doping concentrations >0.5 mg mL^{-1}. The surface temperature was 56.7 and 63.0 °C for the CFNPs$_{0.1}$@Aga and CFNPs$_{0.2}$@Aga aerogels respectively, which supported the saturation hypothesis (Fig. S9†). We speculated that for a higher surface temperature, the heat exchange between the photothermal membrane and the surroundings increased, leading to an increased heat loss. In summary, our designed evaporator was excellent in terms of photothermal conversion, water transportation, and energy utilization, suggesting a suitable device for the subsequent solar-driven interfacial evaporation step.

Solar steam generation and water purification with the CFNPs@Aga aerogel

Having demonstrated the excellent photothermal performance of CFNPs and CFNPs@Aga aerogels, we evaluated the evaporation performance of the evaporator integrating the aerogel using the experimental setup depicted in Fig. 5a. The mass change of the sample was continuously measured using an analytical balance. As the control group, the evaporation rate of pure water was 0.37 kg m^{-2} h^{-1} (Fig. 5b). The aga aerogel membrane showed an elevated, yet still moderate, evaporation rate of 1.87 kg m^{-2} h^{-1}. When equipped with the CFNPs@Aga aerogel membrane, the evaporation rate was greatly promoted to 2.59 and 3.06 kg m^{-2} h^{-1}, depending on the doping concentration of CFNPs (0.5 and 1.0 mg mL^{-1}, respectively). We hypothesized that the higher evaporation rate of the CFNPs$_{1.0}$@Aga aerogel originated from its higher loading of CFNPs, which created stronger interactions with the evaporating water molecules and hence lower evaporation enthalpy.

The CFNPs@Aga aerogel membrane exhibited favourable cycling performance and durability during repeated use. The evaporation rate of 5.0 wt% NaCl solution showed no obvious decay in three independent evaporation processes using the same piece of aerogel membrane (Fig. S10†). Additionally, the macroscopic integrity of the membrane remained unchanged. Thus, the photothermal CFNPs@Aga aerogel had a potential in evaporation-driven water purification.

We next used solutions of NaCl, Eriochrome black T (EBT), and *P. aeruginosa* to mimic seawater, dyeing wastewater, and
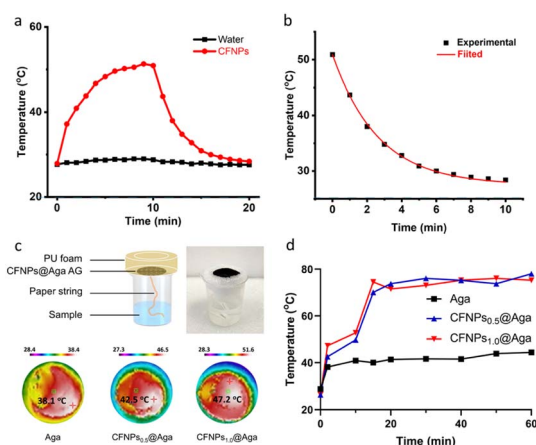

Fig. 4 Photothermal conversion performance of CFNPs and CFNPs@Aga aerogels. (a) Temperature increase profiles of CFNPs and water under 808 nm laser irradiation. (b) Cooling curve of CFNPs used for calculating the photothermal conversion efficiency. (c) Schematic illustration and photograph of the interfacial evaporator. IR images of the evaporation interface after 2 min of irradiation. (d) Temperature curves of the evaporation interface under 1 sun irradiation.
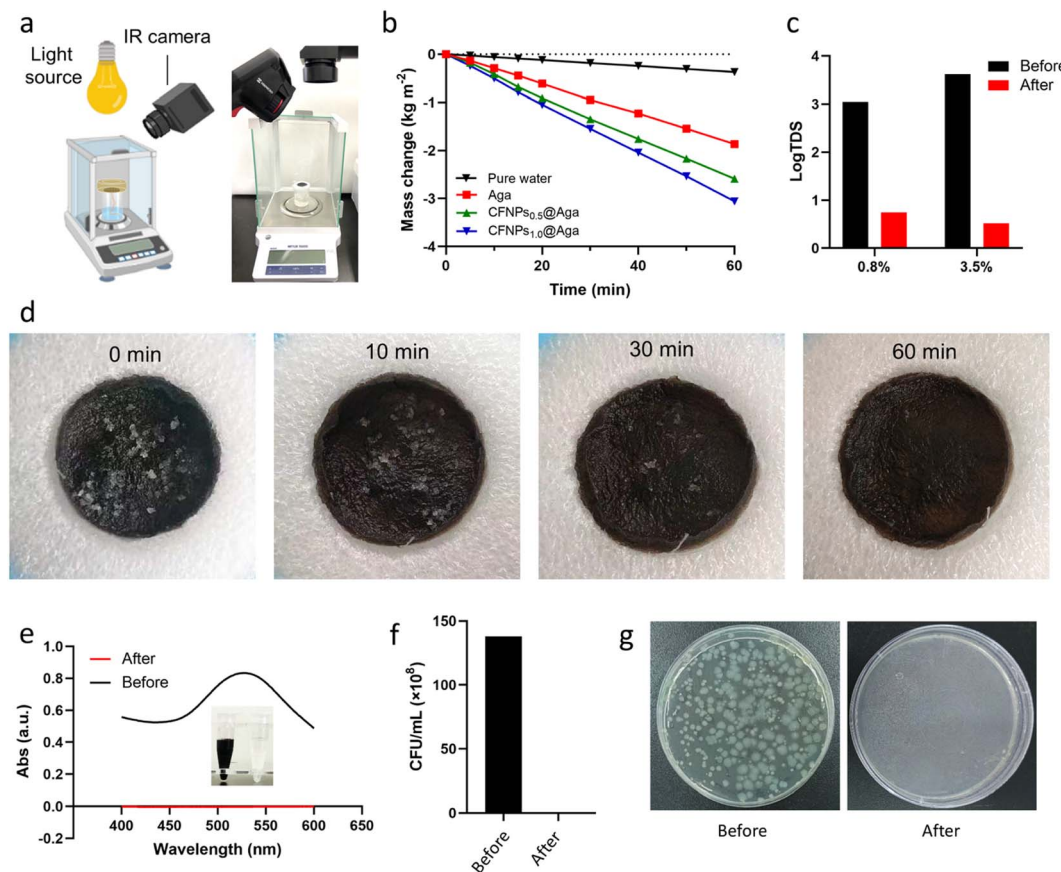
Fig. 5 Evaluation of the solar-driven evaporation performance of the CFNPs@Aga aerogel. (a) Experimental setup to measure the evaporation rate. (b) Mass changes of water for evaporators equipped with different aerogel membranes, with pure water as a control. (c) TDS of NaCl solutions with different concentrations before and after being treated with the evaporator. (d) Anti-salt-fouling performance of the CFNPs@Aga aerogel. (e) UV-Vis spectra and photographs of the EBT solutions before and after being treated with the evaporator. (f and g) Bacterial colony counting (f) and bacterial cell culture (g) of *P. aeruginosa* suspensions before and after treatment.

bacteria-contaminated water, respectively, to show the potential of our device for obtaining freshwater from seawater and sewage. The experimental setup is shown in Fig. S11.† We measured the total dissolved solids (TDS) in the solution to characterize the salinity of the pristine NaCl solution and the condensate water collected after the interfacial evaporation. As shown in Fig. 5c, the TDS of the NaCl solution decreased by 3 orders of magnitude after evaporation and condensation, indicating successful desalination of the sample. Salt fouling poses a severe challenge to interfacial evaporation devices because the precipitated salt (*e.g.*, NaCl) can block the evaporation channels and even destroy the skeletons of the device.[26] We studied the salt self-cleaning performance of the CFNPs@Aga aerogel by exposing the evaporation device to 0.1 g of NaCl crystals. The salt solids quickly dissolved back to the bulk solution in 1 h due to the high solubility of NaCl in water (35.7 mg mL^{-1}) and the porous structure of the aerogel (Fig. 5d). We thus expected that the CFNPs@Aga aerogel would be suitable for seawater desalination with a long working life.

We also demonstrated the applicability of the evaporator in the treatment of dye- and bacteria-contaminated sewage. The freshwater obtained from the deep purple EBT solution was colorless in appearance with no absorption at the characteristic

peak position of 530 nm, indicating there was no residual dye in the purified water (Fig. 5e). Additionally, the plating counting results showed that no live bacteria existed in the sample obtained from purifying the water contaminated with *P. aeruginosa* (Fig. 5f and g). Overall, the favorable evaporation performance of the CFNPs@Aga aerogel membrane made it applicable for extracting freshwater from various samples.

Efficiency, cost effectiveness, and ecological impact of the evaporator

Hydrogels are known to facilitate water evaporation by interacting with water molecules in their 3D networks and reducing the evaporation enthalpy (ΔH_{vap}) of water. We anticipated that the hydrophilic skeletons of the CFNPs@Aga aerogel would contribute to strong interactions with water molecules and thus lead to enhanced evaporation rates with reduced ΔH_{vap}. We applied differential scanning calorimetry (DSC) to measure the ΔH_{vap} of pure water and the CFNPs@Aga aerogel. The ΔH_{vap} of the aerogel was 1053.39 J g^{-1}, which is much lower than that of pure water (1547.46 J g^{-1}) (Fig. 6a). Based on the ΔH_{vap}, we calculated the light-to-vapor energy efficiency (η) of the evaporator using the following equation
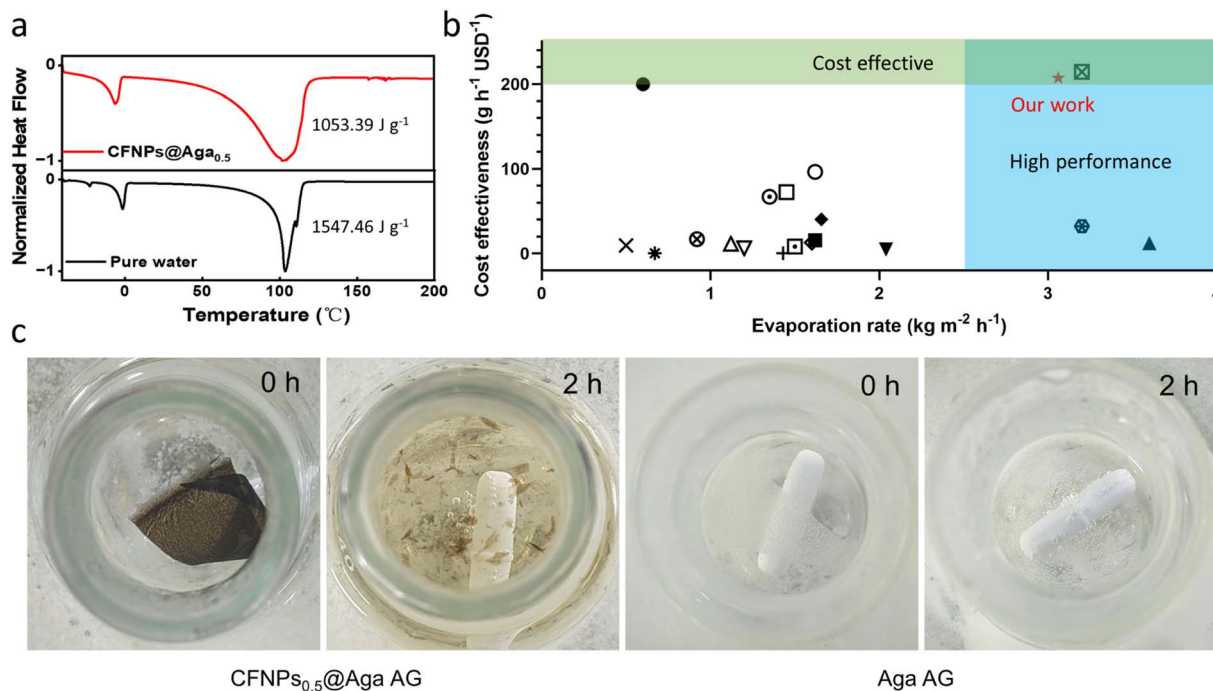
Fig. 6 Efficiency, cost effectiveness, and degradability of the CFNPs@Aga aerogel. (a) DSC curves of pure water and the aerogel. (b) Cost effectiveness of the CFNPs@Aga aerogel. (c) Degradability of the CFNPs@Aga aerogel. Pictures show the CFNPs@Aga and pure aga aerogels in NaOH solution before and after heating.

$$\eta = \frac{m(\Delta H_{\text{vap}} + Q)}{P_{\text{in}}}$$

where m is the water evaporation rate (after subtraction of the dark evaporation of the samples, which was 0.37 kg m^{-2} h^{-1}), ΔH_{vap} is the phase change enthalpy, Q is the sensible heat of water, and P_{in} is the input solar irradiation power (1 kW m^{-2}). The efficiency of the aerogel was calculated to be 94.91%.

Cost effectiveness is an important claim of green chemistry. In our study, the cost-effectiveness of the evaporation device was calculated as $\varepsilon = r/c$, where r was the evaporation rate (kg m^{-2} h^{-1}), and c was the materials cost ($ per m^2).[27] The value of ε represented how many grams of freshwater could be obtained in 1 h for a cost of one U.S. dollar. The raw materials we used to prepare the aerogel, cuttlefish ink and aga powder, are both readily available marine resources. The CFNPs@Aga aerogel membrane showed a high ε value of 192 g h^{-1} per USD, which was superior to that of many other reported evaporators (Fig. 6b and Tables S1 and S2†). Thus, the CFNPs@Aga aerogel offered both a high evaporation rate and high cost-effectiveness.

Evaporators made of synthetic chemicals like plastics, sponges, metals, *etc.*, generally suffer from poor degradability in the environment. In our device, both CFNPs and aga are natural polymer products, *i.e.*, melanin and polysaccharide, respectively, meaning that the composite aerogel had good degradability with nontoxic products.[28] It has been reported that hot alkaline solution can degrade aga[29] as well as melanin.[30] We thus immersed the CFNPs@Aga aerogel in 1 M sodium hydroxide (NaOH) and heated the mixture to 80 °C. The membrane rapidly degraded into small pieces after 2 h,

accompanied by the solution becoming yellowish (Fig. 6c). The colour change of the solution was basically due to the degradation of CFNPs into phenol/quinone monomers, because the degradation of the pure aga aerogel resulted in a colourless solution. Therefore, unlike many other evaporators, the CFNPs@Aga aerogel membrane was easily degradable and thus was much greener in real use.

To further assess the ecological impact of the composite aerogels, we incubated domestic *Poecilia reticulata* with the different samples (aga membrane, CFNPs@Aga membrane, and CFNPs solution) to study their aquatic toxicity. The fish in all groups remained active during a 7 day culture period, meaning that both aga and CFNPs were safe to aquatic animals (Fig. S12†). Additionally, we studied the natural degradation behaviour of the CFNPs@Aga membrane in the soil and found that a degradation efficiency of 14.2% was achieved after 14 days (Table S3†). Therefore, the composite aerogel was safe to the environment with good degradability.

Desalination of real seawater samples

We tested the performance of the evaporator in the desalination of real samples of seawater. Fig. 7a depicts the experimental device used to obtain freshwater from seawater, in which the evaporator was supported in the middle part of a sealed container to allow the condensed water to flow down into the collector. The device was placed outdoors under sunlight, and the mass change, solar intensity, and air temperature were continuously monitored. As shown in Fig. 7b, the device achieved a freshwater production of 3.6 L m^{-2} in the daytime in the
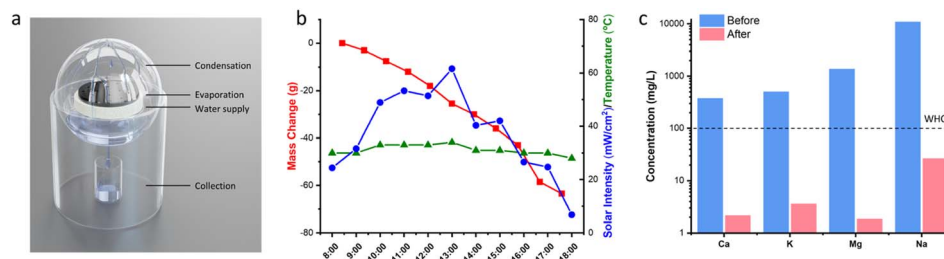
Fig. 7 Seawater desalination using real samples. (a) Experimental setup for the desalination of real seawater. (b) Mass change, solar irradiation intensity, and air temperature curves monitored during the desalination process. (c) Concentrations of various cations in the samples before and after desalination.

presence of an average solar intensity of 374 W m^{-2} (∼0.3 sun irradiation). According to the drinking water guidelines of the World Health Organization (WHO), the suitable concentrations of Ca^{2+} and Mg^{2+} in drinking water are 10–50 mg L^{-1}. We used inductively coupled plasma-optical emission spectroscopy (ICP-OES) to measure the concentrations of various cations (Ca^{2+}, K$^+$, Mg^{2+}, Na$^+$) in the samples before and after treatment. After desalination, the concentration of each ion decreased by two (for Ca^{2+}, K$^+$, Na$^+$) or three orders of magnitude (for Mg^{2+}), reaching the standard for preparing drinking water (Fig. 7c). Thus, the CFNPs@Aga aerogel had great potential for seawater desalination to obtain fresh drinking water.

Conclusions

In summary, a biomass-derived CFNPs@Aga aerogel was designed as a solar absorber for solar steam generation. The aerogel was easy to fabricate, cost-effective, and degradable. The evaporation device achieved a high evaporation rate of 3.06 kg m^{-2} h^{-1} with an energy efficiency of 94.91%, which makes it potentially applicable in seawater desalination and sewage treatment. Our work offers a facile route toward a sustainable solar evaporator for interface evaporation. In the future, the CFNPs can be further modified to implement complicated roles, which is expected to bring multifunctionality to the designed evaporator for advanced environmental applications.

Author contributions

Yong Liu – conceptualization, funding acquisition, investigation, writing – original draft; Ruyue Wang – investigation, data curation, formal analysis; Kaiyuan Wang – investigation, data curation; Fei Yang – investigation, validation; Yundi Chen – investigation; Wenwen Xie – investigation; Shengxu Luo – funding acquisition, writing – review & editing; Zhenyi Liang – investigation, data curation; Qian Wang – conceptualization, writing – review & editing; Juanjuan Li – conceptualization, funding acquisition, writing – review & editing.

Conflicts of interest

There are no conflicts to declare.

Acknowledgements

Notes and references

1 P. Tao, G. Ni, C. Song, W. Shang, J. Wu, J. Zhu, G. Chen and T. Deng, *Nat. Energy*, 2018, **3**, 1031–1041.

2 M. S. Irshad, N. Arshad, M. S. Asghar, Y. Hao, M. Alomar, S. Zhang, J. Zhang, J. Guo, I. Ahmed, N. Mushtaq, M. A. K. Y. Shah, L. Noureen, S. Wageh, O. A. Al-Hartomy, A. Kalam, V.-D. Dao, H. Wang, X. Wang and H. Zhang, *Adv. Funct. Mater.*, 2023, 2304936.

3 L. Zhou, Y. Tan, D. Ji, B. Zhu, P. Zhang, J. Xu, Q. Gan, Z. Yu and J. Zhu, *Sci. Adv.*, 2016, **2**, e1501227.

4 J. Li, L. Yan, X. Li, W. Song and Y. Li, *J. Environ. Chem. Eng.*, 2022, **10**, 107690.

5 M. U. Farid, J. A. Kharraz, P. Wang and A. K. An, *J. Cleaner Prod.*, 2020, **271**, 122684.

6 R. Mehrkhah, M. Mohammadi, A. Zenhari, M. Baghayeri and M. R. Roknabadi, *Ind. Eng. Chem. Res.*, 2022, **62**, 4573–4586.

7 M. S. Irshad, Y. B. Hao, N. Arshad, M. Alomar, L. Y. Lin, X. Q. Li, S. Wageh, O. A. Al-Hartomy, A. G. Al-Sehemi, V. D. Dao, H. Wang, X. B. Wang and H. Zhang, *Chem. Eng. J.*, 2023, **458**, 141431.

8 M. S. Irshad, N. Arshad, J. Zhang, C. Song, N. Mushtaq, M. Alomar, T. Shamim, V.-D. Dao, H. Wang, X. Wang and H. Zhang, *Adv. Energy Sustainability Res.*, 2023, **4**, 2200158.

9 X. Ming, A. Guo, Q. Zhang, Z. Guo, F. Yu, B. Hou, Y. Wang, K. P. Homewood and X. Wang, *Carbon*, 2020, **167**, 285–295.

10 X. Li, S. Tanyan, S. Xie, R. Chen, Q. Liao, X. Zhu and X. He, *Sep. Purif. Technol.*, 2022, **292**, 120985.

11 Y. Liu, K. Ai, J. Liu, M. Deng, Y. He and L. Lu, *Adv. Mater.*, 2013, **25**, 1353–1359.

12 X. Liu, Y. Tian, Y. Wu, F. Chen, Y. Mu, M. L. Minus and Y. Zheng, *ACS Appl. Mater. Interfaces*, 2021, **13**, 42832–42842.

13 F. Zhao, X. Zhou, Y. Shi, X. Qian, M. Alexander, X. Zhao, S. Mendez, R. Yang, L. Qu and G. Yu, *Nat. Nanotechnol.*, 2018, **13**, 489–495.

14 S. Panja, B. Dietrich and D. J. Adams, *Angew. Chem., Int. Ed.*, 2022, **61**, e202115021.

15 L. Shi, K. Sun, G. Zhang, M. Jiang, X. Xu and X. Zhuang, *J. Colloid Interface Sci.*, 2022, **624**, 377–384.

16 T. Meng, B. Jiang, Z. Li, X. Xu, D. Li, J. Henzie, A. K. Nanjundan, Y. Yamauchi and Y. Bando, *Nano Energy*, 2021, **87**, 106146.

17 J. Rostami, K. Gordeyeva, T. Benselfelt, E. Lahchaichi, S. A. Hall, A. V. Riazanova, P. A. Larsson, G. C. Ciftci and L. Wagberg, *Mater. Today*, 2021, **48**, 47–58.

18 J. Zhou, W. Liu, X. Zhao, Y. Xian, W. Wu, X. Zhang, N. Zhao, F.-J. Xu and C. Wang, *Adv. Sci.*, 2021, **8**, 2100505.

19 S. Maher, M. Mahmoud, M. Rizk and H. Kalil, *Environ. Sci. Pollut. Res.*, 2020, **27**, 19115–19126.

20 Z. Lin, L. Liu, W. Wang, L. Jia, Y. Shen, X. Zhang, D. Ge, W. Shi and Y. Sun, *Biomater. Sci.*, 2021, **9**, 5951–5964.

21 J. Dong, J. Sun, W. Cai, C. Guo, Q. Wang, X. Zhao and R. Zhang, *Nanomedicine*, 2022, **41**, 102510.

22 Y. Liu, M. Yang, J. Li, W. Zhang and X. Jiang, *Anal. Chem.*, 2019, **91**, 6754–6760.

23 Q. Lyu, N. Hsueh and C. L. L. Chai, *Langmuir*, 2019, **35**, 5191–5201.

24 Y. Zou, X. Chen, P. Yang, G. Liang, Y. Yang, Z. Gu and Y. Li, *Sci. Adv.*, 2020, **6**, eabb4696.

25 B. Shao, Y. Wang, X. Wu, Y. Lu, X. Yang, G. Y. Chen, G. Owens and H. Xu, *J. Mater. Chem. A*, 2020, **8**, 11665–11673.

26 Y. Zhang, T. Xiong, D. K. Nandakumar and S. C. Tan, *Adv. Sci.*, 2020, **7**, 1903478.

27 Z. Wang, X. Wu, J. Dong, X. Yang, F. He, S. Peng and Y. Li, *Chem. Eng. J.*, 2022, **427**, 130905.

28 A. Awadhiya, D. Kumar, K. Rathore, B. Fatma and V. Verma, *Polym. Bull.*, 2017, **74**, 2887–2903.

29 R. L. Whistler and J. N. Bemiller, *Adv. Carbohydr. Chem.*, 1958, **13**, 289–329.

30 S. Ito and K. Wakamatsu, *Pigm. Cell Res.*, 1998, **11**, 120–126.